Heavy fragment production cross sections from 1.05 GeV/nucleon ^{56}Fe in C, Al, Cu, Pb, and CH$_2$ targets

C. Zeitlin,[1] L. Heilbronn,[1] J. Miller,[1] S. E. Rademacher,[2] T. Borak,[2] T. R. Carter,[3] K. A. Frankel,[1] W. Schimmerling,[4] and C. E. Stronach[3]

[1]*Lawrence Berkeley National Laboratory, Berkeley, California 94720*
[2]*Department of Radiological Health Sciences, Colorado State University, Fort Collins, Colorado 80523*
[3]*Department of Physics, Virginia State University, Petersburg, Virginia 23806*
[4]*National Aeronautics and Space Administration, Washington, DC 20546*

We have obtained charge-changing cross sections and partial cross sections for fragmentation of 1.05 GeV/nucleon Fe projectiles incident on H, C, Al, Cu, and Pb nuclei. The energy region covered by this experiment is critical for an understanding of galactic cosmic ray propagation and space radiation biophysics. Surviving primary beam particles and fragments with charges from 12 to 25 produced within a forward cone of half-angle 61 mrad were detected using a silicon detector telescope to identify their charge and the cross sections were calculated after correction of the measured yields for finite target thickness effects. The cross sections are compared to model calculations and to previous measurements. Cross sections for the production of fragments with even-numbered nuclear charges are seen to be enhanced in almost all cases. [S0556-2813(97)00907-2]

PACS number(s): 25.75.−q, 98.70.Sa

I. INTRODUCTION

Heavy-ion fragmentation has been the subject of much experimental and theoretical work, yet there remain considerable discrepancies both between experiments and models as well as between experiments which purport to measure the same things. The fragmentation of the high-energy heavy-ion component of the galactic cosmic rays (GCR) has applications in astrophysics [1] and in radiobiology and radiation protection. A precise and accurate description of the transport of heavy ions in matter, which is sensitive to details of fragmentation, is essential in understanding the effects of the heavy-ion component of the GCR on humans in space [2]. The heaviest ion present in significant numbers in the GCR is ^{56}Fe; the measurements described in this paper were made with iron ions at an energy of 1.05 GeV/nucleon, which is near the peak of the solar-modulated GCR iron energy spectrum [3]. While many results have been published on iron fragmentation between several hundred MeV/nucleon and several GeV/nucleon [4–10], previously-reported fragment production cross sections [4,7,9] show significant discrepancies which we believe are resolved by the present measurements.

II. EXPERIMENTAL APPARATUS

The data reported here were obtained during experiment E898 at the Alternating Gradient Synchrotron (AGS) at Brookhaven National Laboratory. A silicon detector telescope, four elements of which were placed upstream of the target, was used to identify charged particles. A very similar system has previously been described in the literature [11]. The arrangement of the detectors used in the present analysis is shown schematically in Fig. 1. Off-line cuts using the detectors upstream of the target allow us to ensure that each event used in the analysis was initiated by a single incident iron ion. The two detectors furthest upstream (T1 and T2) were each about 330-μm thick with active areas of 300 mm^2, and were used to trigger the experiment. All silicon detectors were read out with standard electronics—a locally mounted charge preamplifier, a shaping amplifier, and an 11- or 12-bit digitizer. A pair of position-sensitive silicon detectors (PSD1Y and 1X), oriented so as to provide vertical and horizontal position information, respectively, were placed downstream of the trigger detectors. Each PSD is $\sim$1-mm thick and has an active area of $\sim$1500 mm^2. Targets were placed immediately downstream of PSD1X; the beam energy at the target entrance was determined (see below) to be 1.053±0.005 GeV/nucleon. A second PSD pair, 2Y and 2X, was placed 30 cm further downstream. Each PSD generates two position-dependent signals and a third signal proportional to the total charge liberated in the detector. In the present analysis we have used only the energy loss, ΔE, signals. The resolution in ΔE was sufficient to allow us to identify obvious peaks in the spectra corresponding to fragment charges as low as 10 or 11 in most cases.

The beam energy at the exit of the vacuum line was determined by two independent methods to be 1.064
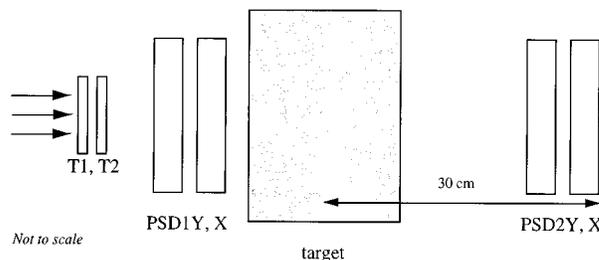

FIG. 1. Schematic diagram showing the relative sizes, depths, and positions of the target and detectors used in the present analysis.
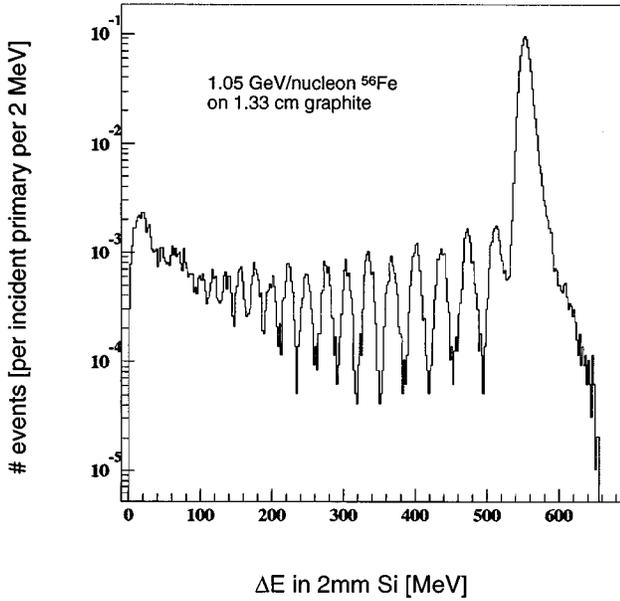
FIG. 2. Histogram of deposited energy in detectors PSD2X and 2Y, with 1.33 cm of graphite in the beam. The combined depth of the two silicon detectors is approximately 2 mm.

± 0.005 GeV/nucleon. The first method used parallel-plate ionization chambers and a variable-depth water column to determine the Bragg curve of the beam. Considerable care was taken in the energy measurement to account for the effects of the beam passing through long sections of air and through the plastic windows on the water column. The second method used the measured shifts in the iron peak location as a function of target depth. The two analyses yielded highly consistent results. The decrease in energy to the quoted value of 1.053 ± 0.005 GeV/nucleon at the target entrance is due to ionization energy loss in the silicon detectors T1, T2, PSD1Y, and PSD1X.

The experimental acceptance is defined by PSD2X. As seen from a point at the target center and precisely on the beam axis, this corresponds to a cone of half-angle 3.5°. Calculations using a Goldhaber-type model for the fragment transverse momentum distributions [12,13] indicate that for the range of fragment charges considered here ($12 \leq Z_{frag} \leq 25$), acceptance corrections are negligible.

III. DATA ANALYSIS

Analysis of the data proceeds in the following steps.

(i) A scatter plot of $\Delta E(T2)$ vs $\Delta E(T1)$ is made, and a cut is made by eye to select events which are within about 2 standard deviations of the iron peak in both detectors. The procedure is repeated using PSD1Y and PSD1X to guarantee that the particle entering the target was iron.

(ii) A scatter plot is made for $\Delta E(PSD2X)$ vs $\Delta E(PSD2Y)$, and events in which a particle undergoes a nuclear interaction in one detector or the other are rejected. Typically, about 3–4 % of events are rejected at this stage.

(iii) A one-dimensional histogram of $\Delta E(PSD2X) + \Delta E(PSD2Y)$ of the events passing the first two cuts is made (see Fig. 2 for an example). Peaks for elements with $Z=12$ to $Z=26$ are evident in all cases; with some thick targets, peaks corresponding to lower Z's are seen.

(iv) In the one-dimensional histogram, the bottom of each "valley" is used to delimit the range of ΔE corresponding to a particular Z. The number of events of a given Z is then determined simply by counting events between the delimiting cuts. [The number $N(Z)$ determined this way differs slightly from that determined by the method of fitting a Gaussian to the peak. In most cases, there was no significant difference between the two. For thin targets and Z from about 12 to 16, the "valleys" are less distinct; in such cases, the parameters from the Gaussian fits to the peaks were used to determine $N(Z)$.] This number, divided by the total number of events in the histogram, defines the probability for finding charge Z, i.e., $P(Z)=N(Z)/N(\text{total})$.

Data taken without a target are used to determine the background for each fragment Z as well as the probability for iron to survive these cuts. We refer to the probabilities thus obtained as $P_0(Z)$, the subscript 0 referring to the absence of a target. These probabilities varied over time, owing to variations in the amount of material on the beamline; in general, runs were corrected using the target-out data taken closest in time, typically within a few hours. For some runs, a tissue-equivalent proportional counter (TEPC) was placed on the beamline between the target and PSD2. When present, the TEPC was the principal source of background, as its materials represent about 3.5% of an interaction length for iron ions. With the TEPC off the beamline, background events comprised less than 1% of the total. The total charge-changing cross section for a given target of depth d can be written

$$\sigma_{cc} = \frac{-A \ln[P_{corr}(26)]}{\rho d N_a}, \qquad (1)$$

where N_a is Avogadro's number, ρ the target density, A the target's mass number, and $P_{corr}(26)=P(26)/P_0(26)$. The error in σ_{cc} is given by

$$\frac{\delta\sigma_{cc}}{\sigma_{cc}} = -\frac{\delta P_{corr}(26)}{P_{corr}(26)} \frac{1}{\ln[P_{corr}(26)]}. \qquad (2)$$

When $P_{corr}(26)$ is close to 1 (the case in thin target data), the error in σ^{cc} is very sensitive to small uncertainties in $P_{corr}(26)$.

The production probability $P(Z)$ for each fragment charge must be corrected for background according to the relation $P_{corr}(Z)=P(Z)-P_0(Z)P_{corr}(26)$. Fragment production cross sections are given by $\sigma_z=\sigma_{cc}\{P_{corr}(Z)/[1-P_{corr}(26)]\}$. Using these formulas, the sum of the fragment production cross sections is equal (as it must be) to the charge-changing cross section.

IV. CORRECTIONS FOR FINITE TARGET DEPTHS

In any target, there is a finite probability for secondary- and higher-generation interactions involving fragments. While these have no effect on the measurement of charge-changing cross sections, they affect fragment yields by depleting the number of fragments with charge close to the primary and enhancing the number of much lighter fragments. To estimate the effects in various data sets, a Monte

Carlo program was written which simulates up to five generations of interactions in a target, and then reports the apparent cross section and the input cross sections. The ratio of the input to apparent cross section provided a unique correction factor for each combination of fragment charge, target material, and target thickness. After the correction factors are applied, one can combine cross sections determined at different depths of a given material, which enhances the statistical accuracy of the measurement and also provides a test of any systematic errors that might arise from the corrections.

Two models for fragment production cross sections were used as input to the Monte Carlo. One was adapted from NUCFRG2, a semiempirical nuclear fragmentation model [14], and the other was a naive model in which all fragments are produced with equal probability (i.e., if a fragment of charge $Z+1$ interacts, the probability for producing any possible secondary fragment is simply $1/Z$). The naive model was used to test the sensitivity of the final results to the cross sections used in this step of the analysis. For this application, we found very little difference between the two models; the respective correction factors in all cases agreed to within 2.5%.

In both NUCFRG2 and the naive model, the probability for a particle to undergo a charge-changing nuclear interaction was determined from its geometric cross section, as parametrized by Townsend and Wilson [15],

$$\sigma(A_1,A_2) = \pi r_0^2 (A_1^{1/3} + A_2^{1/3} - 0.2 - A_1^{-1} - A_2^{-1})^2, \quad (3)$$

where $r_0 = 1.26$ fm and A_1, A_2 refer to the mass numbers of the colliding nuclei. Note that the geometric cross section is larger than the charge-changing cross section, since the former includes reactions in which only neutrons are stripped from the projectile. As will be discussed further, there are many other parametrizations of the geometric cross section, and they generally yield results that are mutually consistent within $\pm 10\%$. This uncertainty represents a separate contribution to the correction factors, e.g., a 10% correction factor has a $\pm 1.0\%$ uncertainty from this error source. Since our correction factors are at most 16%, we estimate that this source contributes an uncertainty of at most 1.6% to the fragment production cross sections.

V. CHARGE-CHANGING CROSS SECTION RESULTS

Table I shows the charge-changing cross sections for iron on hydrogen, carbon, polyethylene, aluminum, copper, and lead targets. The hydrogen cross section is inferred from the carbon and polyethylene data according to the relation $\sigma_H = 0.5(\sigma_{CH_2} - \sigma_C)$. The relative error on the hydrogen measurement is large compared to the other targets, owing to the propagation of errors in the CH_2 and C cross sections. The errors for any individual target depth are statistical only. (In determining the uncertainty in the surviving iron fraction in any given sample, it is proper to treat the errors as binomial.) In the fifth column from the left, we show the weighted average cross sections determined by combining results from all target depths of a given material. For each material, the spread in σ_{cc} determined at different depths is less than or approximately equal to 2.5% of the weighted average value. We interpret this spread as arising from systematic errors in

TABLE I. Total charge-changing cross sections for ^{56}Fe on various targets, in millibarns. The errors are statistical only on the individual target results, with a 2.5% systematic error assigned to the weighted average results. The hydrogen cross section is inferred from the measured C and CH_2 cross sections.

Target	σ_{cc} (mb) (Depth)	σ_{cc} (mb) (Depth)	σ_{cc} (mb) (Depth)	σ_{cc} (mb) wtd. av.
H				661±40
C	1423±13 (1.33 cm)	1520±7 (2.66 cm)		1496±37
CH$_2$	2809±11 (2.16 cm)	2823±8 (5.20 cm)		2818±70
Al	2072±14 (0.65 cm)	2074±9 (1.30 cm)	1967±9 (2.60 cm)	2010±50
Cu	2779±15 (0.32 cm)	2870±9 (0.64 cm)	2731±8 (1.28 cm)	2789±70
Pb	4185±18 (0.3175 cm)			4185±107

our methodology and, in the weighted average column, the quoted error is the quadrature sum of the statistical and systematic errors (with the latter dominating). We note that the fragment production cross sections are proportional to the charge-changing cross sections, and therefore any systematic error in the latter propagates to the systematic error in the former.

A number of parametrizations of the energy-independent charge-changing cross section exist. In a recent paper [16], Nilsen *et al.* review several of them. Their best-fit form uses nuclear radii measured via electron scattering (multiplied by a scale factor determined from their data), and is expressed as

$$\sigma(R_P, R_T) = \pi[R_P + R_T - \Delta R]^2, \quad (4)$$

where R_p and R_T are the (scaled) radii of the projectile and target, respectively, and the overlap term ΔR is experimentally found to be 3.20 ± 0.05 fm. Calculated values using Eq. (4) are shown in Table II, along with values determined from the Bradt-Peters form [17] using parameters determined by Chen *et al.* [1] ($r_0 = 1.35$ fm, and the overlap parameter $b = 0.83$). Also shown in the table are predictions from the NUCFRG2 code [14] and from the QMSFRG code [18]. We show values of χ^2 along with the model predictions. Equation (4) gives a χ^2 per degree of freedom of 3.8; the Bradt-Peters form, 5.1; NUCFRG2, 8.2; and QMSFRG 13.6. The first three values are comparable to those reported in Ref. [16] with somewhat heavier beam ions (^{84}Kr and ^{109}Ag). Except for the hydrogen target result, the measured cross sections are smaller than predicted by most or all of the models.

VI. FRAGMENT PRODUCTION CROSS SECTIONS

In the preceding discussion, we have identified three sources of systematic error which apply to all fragment production cross sections: (i) the fragmentation model used to determine the target thickness corrections, 2.5%; (ii) the geometric cross sections used in the Monte Carlo, 1.6%; (iii) the propagated errors from σ_{cc}, about 2.5%. Added in quadra-

TABLE II. Charge-changing cross sections as per Table I, compared to several models.

Target	σ_{cc} (mb) wtd. av.	σ_{cc} (mb) Eq. (4) (Nilsen)	χ^2	σ_{cc} (mb) (Bradt-Peters)	χ^2	σ_{cc} (mb) NUCFRG2	χ^2	σ_{cc} (mb) QMSFRG	χ^2
H	661±40	584	3.7			659	0.0		
C	1496±37	1522	0.5	1599	7.7	1630	13.1	1613	10.0
Al	2010±50	1902	4.7	2058	0.9	2101	3.3	2202	14.7
Cu	2789±70	2841	0.6	2802	0.1	2833	0.4	2995	8.7
Pb	4185±107	4509	9.5	4547	11.5	4608	15.8	4672	20.9

ture, these total about 4%.

Data taken with varying depths of a given target material allow us to make multiple independent measurements of the fragment production cross sections. After the target thickness corrections have been applied, the cross sections measured at different depths of a given material should be mutually consistent within the statistical and systematic errors. If the measurements are consistent with one another (as determined by evaluating the χ^2), it is then reasonable to take as our ''best measurement'' the weighted average of the multiple measurements. In Table III, we show the weighted average obtained with the two carbon-target data sets. The χ^2, which is a measure of how well the data sets agree, is 14.3 for 14 degrees of freedom, which suggests that it is reasonable to

have combined the data sets. The errors shown in the table are quadrature sums of statistical and systematic uncertainties. Tables IV–VII show analogous results for aluminum, copper, lead, and hydrogen targets. In Tables VI and VII, there is no combining of data sets and therefore no χ^2 to report. Summing over all the χ^2's reported in Tables III–V yields a total of 58.9 for 70 degrees of freedom; the probability for χ^2 to exceed this value is 80%. If the target thickness corrections were introducing substantial errors, the result would be large values of χ^2; the very reasonable values obtained suggest that the corrections have been determined within the quoted accuracy. (Indeed, the high probability to exceed this value of χ^2 suggests that, if anything, the systematic errors may be slightly overestimated.)

A. Odd-even effect

For all targets, the fragment production cross sections do not fall monotonically with increasing charge-change ΔZ.

TABLE III. Cross sections in millibarns, after corrections, for iron on carbon targets. The weighted average cross section, obtained from data taken at two target depths, is shown alongside results from previous experiments. The uncertainties shown for the present experiment are the quadrature sums of statistical and systematic errors. The total χ^2 for combining data sets obtained in the present experiment is 14.3 for 14 degrees of freedom.

TABLE IV. Results as per Table III, for data taken with three depths of aluminum targets. The total χ^2 for combining data sets obtained in the present experiment is 18.6 for 28 degrees of freedom.

	σ(mb) this experiment	Westfall et al. (mb)	Cummings et al. (mb)	Webber et al. (mb)
σ_{25}	152±6	181±27	141±3	158±2
σ_{24}	114±5	124±13	105±3	113±2
σ_{23}	75±3	100±11	79±2	78±2
σ_{22}	78±4	87±11	75±2	76±2
σ_{21}	61±3	54±9	57±2	56±2
σ_{20}	62±3	78±11	63±2	58±2
σ_{19}	45±2	52±7	44±2	41±2
σ_{18}	50±2	55±9	48±2	42±2
σ_{17}	42±2	53±7	41±2	35±2
σ_{16}	48±2	54±10	46±2	41±2
σ_{15}	40±2	59±10	39±2	29±3
σ_{14}	53±2	57±10	51±2	44±4
σ_{13}	42±2	83±11	41±2	27±3
σ_{12}	51±2		45±2	36±4

	σ(mb) this experiment	σ(mb) Cummings et al.
σ_{25}	181±6	174±4
σ_{24}	124±5	128±3
σ_{23}	90±4	91±3
σ_{22}	93±4	84±3
σ_{21}	72±3	73±2
σ_{20}	74±3	69±2
σ_{19}	59±3	53±2
σ_{18}	59±2	53±2
σ_{17}	49±2	45±2
σ_{16}	55±2	52±2
σ_{15}	48±2	43±2
σ_{14}	67±3	58±2
σ_{13}	44±2	45±2
σ_{12}	56±3	52±2

TABLE V. Results as per Tables III and IV, for data taken with three depths of copper targets. The total χ^2 for combining data sets obtained in the present experiment is 25.9 for 28 degrees of freedom.

	σ(mb) this experiment	σ(mb) Cummings *et al.*	σ(mb) Westfall *et al.*
σ_{25}	232±9	239±7	219±20
σ_{24}	154±6	147±4	149±16
σ_{23}	112±5	99±3	121±15
σ_{22}	112±5	98±3	101±14
σ_{21}	84±4	74±3	100±15
σ_{20}	85±4	80±3	98±14
σ_{19}	65±3	60±2	88±14
σ_{18}	69±3	61±2	95±15
σ_{17}	65±3	49±2	86±13
σ_{16}	65±3	60±2	56±11
σ_{15}	60±3	50±2	88±15
σ_{14}	73±4	72±2	72±11
σ_{13}	57±3	51±2	179±27
σ_{12}	71±3	61±2	

TABLE VI. Results as per Tables III–V, for data taken with a single lead target.

	σ(mb) this experiment	σ(mb) Cummings *et al.*	σ(mb) Westfall *et al.*
σ_{25}	481±31	501±13	509±40
σ_{24}	203±17	223±6	242±25
σ_{23}	146±13	130±5	142±20
σ_{22}	137±12	135±5	148±22
σ_{21}	107±11	104±4	111±17
σ_{20}	112±11	98±4	144±22
σ_{19}	99±10	80±4	90±19
σ_{18}	86±9	77±4	73±15
σ_{17}	80±9	60±3	90±19
σ_{16}	63±8	76±3	116±19
σ_{15}	74±8	64±3	78±16
σ_{14}	90±9	86±4	119±22
σ_{13}	76±19	62±3	191±37
σ_{12}	77±19	74±3	

TABLE VII. Cross sections in millibarns, after corrections, for iron on a hydrogen target, alongside results from previous experiments. The cross sections are inferred using data taken with polyethylene and carbon targets, as described in the text.

	σ(mb) this experiment	σ(mb) Webber *et al.*	σ(mb) Westfall *et al.*
σ_{25}	111±7	110±3	127±24
σ_{24}	93±6	87±3	80±13
σ_{23}	73±4	66±2	60±11
σ_{22}	74±4	70±2	82±13
σ_{21}	55±3	52±2	62±11
σ_{20}	51±3	52±2	47±11
σ_{19}	40±3	36±2	36±9
σ_{18}	36±3	34±2	31±9
σ_{17}	28±2	22±2	36±17
σ_{16}	25±2	27±3	37±24
σ_{15}	17±2	15±3	22±10
σ_{14}	21±2	20±4	31±9
σ_{13}	14±2	13±3	25±10
σ_{12}	8±2		

Instead, enhanced production of even-Z nuclei (the ''odd-even effect''), particularly silicon ($Z=14$), is seen. Aside from $\Delta Z=1$ and 2, the cross sections for production of even-Z nuclei Z_{ev} are seen to be comparable to or larger than the cross sections for the species with charges ($Z_{ev}+1$), and significantly larger than the cross sections for the species with charges ($Z_{ev}-1$). Similar behavior has recently been noted in fragmentation cross sections at slightly lower beam energies for heavy ions with isospin $T_z=0$ on hydrogen targets by Knott *et al.* [19]; the enhancement of silicon production is attributed to its shell structure (closed $d_{5/2}$ subshell). The authors of Ref. [19] note that their data show a clear odd-even effect when the incident projectile has isospin $T_z=0$, and no such effect when $T_z=-2$. However, ^{56}Fe has $T_z=-2$ and, in the present data, an odd-even effect is seen for several targets, apparently including hydrogen, as discussed below.

In order to quantify the odd-even effect, and to look for any dependence of the effect on target mass, we define for even-Z species the ratio $\sigma(Z_{ev})/\sigma_{interp}(Z_{ev})$, where the cross section in the numerator is measured and that in the denominator is obtained by interpolating between the cross sections of the adjacent species, i.e.,

$$\sigma_{interp} = \sigma(Z_{ev}-1) + \frac{\sigma(Z_{ev}+1)-\sigma(Z_{ev}-1)}{2}. \quad (5)$$

Ratios were calculated from Tables III–VII, for even Z's between 14 and 22, using data from the present experiment; the results are shown in Table VIII. (We exclude $Z=24$, as

TABLE VIII. The ratio $\sigma(Z_{ev})/\sigma_{interp}(Z_{ev})$ for even-Z nuclei and various targets. The ratios are obtained using the cross sections reported for this experiment in Tables III–VII, using Eq. (5). Values greater than 1.0 indicate an enhancement in the production of even-Z nuclei.

Z_{frag}	Hydrogen	Carbon	Aluminum	Copper	Lead
22	1.16±0.09	1.15±0.09	1.15±0.08	1.14±0.08	1.08±0.15
20	1.07±0.10	1.17±0.09	1.17±0.08	1.14±0.08	1.09±0.17
18	1.06±0.12	1.15±0.08	1.09±0.07	1.06±0.08	0.96±0.16
16	1.11±0.15	1.17±0.09	1.13±0.07	1.04±0.08	0.82±0.15
14	1.35±0.25	1.29±0.09	1.46±0.10	1.25±0.10	1.20±0.24

there is no hint of an enhancement for those cross sections.) The data for carbon, aluminum, and copper targets yield remarkably similar ratios, almost all of which are 1–2 standard deviations above the null result value of 1.0. The ratios obtained for fragment charges 16, 18, 20, and 22 for these targets and for the hydrogen target are mutually consistent within errors, and have a combined weighted average of 1.13±0.02. Combining the ratios for the same targets for $Z=14$ yields a value of 1.33±0.05.

For the lead-target data, the large uncertainties in Table VIII preclude firm conclusions. The central values of the ratios are uniformly lower than for the other targets and all are consistent with a null result.

For the hydrogen target, the values are consistent, within errors, with both the null result and with the data for carbon, aluminum, and copper. However, the weighted average of the ratios for $Z=16$ through 22 is 1.12±.05, significantly away from the null result, and the Webber *et al.* hydrogen-target data—which have smaller uncertainties than the present data for $Z\geqslant18$—show a significant odd-even effect. (Using their data, we find ratios of 1.19±0.06 for $Z=22$, 1.18±0.08 for $Z=20$, and 1.17±0.12 for $Z=18$, results which are, again, significantly above 1.0.) These results suggest that there is an odd-even effect with a $T_z=-2$ projectile and a hydrogen target, which would not have been expected on the basis of the analysis in Ref. [19].

B. Comparison to previous experiments at 1–2 GeV/nucleon

We turn now to a comparison of our data with previous data taken with iron projectiles at beam energies between 1 and 2 GeV/nucleon, where the total charge-changing cross sections for incident iron have been observed to be approximately independent of beam energy [6]. Tables III–VII show cross sections obtained previously by other groups with the same target materials as were used in the present experiment. The beam energies for the previous measurements were as follows: Westfall *et al.* [4], 1.88 GeV/nucleon; Webber *et al.* [6–8], 1.086 GeV/nucleon; Cummings *et al.* [9], 1.55 GeV/nucleon.

For the carbon target, shown in Table III, the present experiment is in excellent agreement with the Cummings *et al.* data, and also with Webber *et al.* over the charge range from 19–25. For charges 18 and below, the Webber *et al.* cross sections are significantly smaller than either the present experiment or the Cummings *et al.* results. The Westfall *et al.* data are—except for $Z=13$—in reasonable agreement with both the present experiment and with Cummings *et al.*

There are previously published data for iron on an aluminum target from Cummings *et al.*, which agree with the present results at about the 10% level, with the Cummings *et al.* cross sections generally smaller than ours. The agreement is somewhat better for charge 19 and above. The results are shown in Table IV.

Previous data for iron on copper (Table V) come from both Cummings *et al.* and Westfall *et al.* and, even excluding the very large disparity at $Z=13$, the two data sets do not agree well. The cross sections reported by Westfall *et al.* tend to be considerably larger, typically 20%, in some cases as great as 50%. For the majority of fragment species, the present data lie in between these two previous data sets. On average, our results are closer to those of Cummings *et al.*, mostly to within about 10%. However, the χ^2 between data sets is actually smallest between our data and that of Westfall *et al.* (This is strongly influenced by the large errors in their data.)

For the lead target data (Table VI), the cross sections previously reported by Cummings *et al.* and by Westfall *et al.* are in reasonable agreement. Our results are in agreement with both, albeit with comparatively large uncertainties. All three experiments find a significant enhancement of the silicon production cross section, however, the present data do not show an enhancement for sulfur ($Z=16$) which is present in the earlier data. As noted above, our data show no statistically significant enhancement for even-Z nuclei between charges 16 and 22 (although the errors are sufficiently large as to not rule out an enhancement). The Cummings *et al.* data, with smaller errors, do appear to show an odd-even effect.

Webber *et al.* and Westfall *et al.* have previously published iron on hydrogen data, which are shown along with our data in Table VII. Over the entire range of fragment charges shown, the present experiment agrees very well with Webber *et al.*—the χ^2 between the two data sets is 11.6 for 14 degrees of freedom. This agreement exists in spite of significant discrepancies between the two experiments in the carbon cross sections for Z from 12 to 18. There are similar discrepancies between the two in this charge range for CH_2 targets (see Table XI). The hydrogen cross sections are (perhaps fortuitously) in good agreement because these discrepancies cancel in the subtraction of the carbon cross sections from the CH_2 cross sections.

To further quantify the comparisons, we define $\Delta\sigma_{av}$ to be the ''average difference'' between previously reported cross sections and the present one for a given target as

$$\Delta\sigma_{av}=\sum_i \left(\frac{\sigma_i(\text{reported})-\sigma_i(\text{present})}{\sigma_i(\text{present})}\right)\bigg/ N_{crs}, \quad (6)$$

where the sum runs over fragment charge i and N_{crs} is the

TABLE IX. Comparison of average differences (the $\Delta\sigma_{av}$ values) and rms's between previous experiments and the present experiment, as described in the text [see Eq. (6)]. For the comparisons to the data of Westfall *et al.*, the first value quoted in each entry is for $13 \leqslant Z_{frag} \leqslant 25$, and the value in parentheses is for $14 \leqslant Z_{frag} \leqslant 25$.

	Cummings		Westfall		Webber	
Target	$\Delta\sigma_{av}$	rms	$\Delta\sigma_{av}$	rms	$\Delta\sigma_{av}$	rms
H			0.16 (0.11)	0.30 (0.24)	-0.060	0.070
C	-0.043	0.043	0.23 (0.17)	0.26 (0.15)	-0.13	0.12
Al	-0.10	0.062				
Cu	-0.099	0.062	0.29 (0.13)	0.59 (0.21)		
Pb	-0.056	0.12	0.25 (0.14)	0.45 (0.26)		
CH$_2$					-0.088	0.077

number of cross sections compared. We use $\Delta\sigma_{av}$ to compare experiments rather than computing χ^2's owing to the large values (and low probabilities, generally less than 1%) obtained in most cases. The large values of χ^2 may be at least partially attributable to the exclusion of systematic errors from previously quoted results. Table IX shows these differences and also shows the root mean square deviations (rms's) of the difference distributions, which are an important measure of the relative scatter in the data sets being compared. Overall, the cross sections reported here agree best with those reported by Cummings *et al.* Not only are the average differences fairly small, the rms's are small. The trends between experiments are obvious: our cross sections are on average about 4–10 % higher than those reported by Cummings *et al.*, with rms's in the range 4–12 %; and our cross sections are 16–29 % lower than those reported by Westfall *et al.*, with significantly larger rms's. Excluding the $Z=13$ data points from the comparisons to Westfall *et al.* reduces the average differences to the range 11–17 %.

From Table IX, one can infer that, even excluding the $Z=13$ points, discrepancies averaging on the order of 20% exist between the Westfall *et al.* and Cummings *et al.* data sets. It is this level of disagreement between previous results which motivates the present set of measurements. Agreement between data and models of better than 10% is considered desirable for use in astrophysical models [19]; clearly, agreement between experiments must be better than this to make the model comparisons meaningful. Also, the determination of required shielding against GCR in spaceflight is very sensitive to uncertainties in fragmentation cross sections [20].

The greatest discrepancy in previous data sets is for fragments with $Z=13$ produced in the copper and lead targets, where in both cases the cross section measured by Westfall *et al.* increases sharply, while that of Cummings *et al.* does not. For these two targets, the Westfall *et al.* data are approximately a factor 3 higher than those of Cummings *et al.*, a trend which persists (although to a lesser extent) in $Z=13$ cross sections with other targets. Our data show no enhancement for $Z=13$.

C. Comparison to models

Figure 3 shows our data for charge-changing cross sections for Fe+H, Fe+C, Fe+Al, Fe+Cu, and Fe+Pb, compared to predictions of four different models. The models are as follows.

(i) The parametrization of Ref. [9] with new parameters determined by Nilsen *et al.* (Eq. (14) of Ref. [16]). Rather than fitting their form to our data to obtain a new set of parameters, we have simply used the parameters as determined from their data to calculate the cross sections shown in the figure. The predictions of this model, which have no explicit Z dependence, are shown as solid lines. On average, the parametrization does well, although significant details are missed: no odd-even effect is predicted, nor are the large cross sections for Si and Mg.

(ii) Cross sections calculated[1] by the method of scaling the corresponding proton-nucleus cross sections [21]. These predictions are shown as curves with large dashes. For the carbon target and $5 \leqslant \Delta Z \leqslant 11$, the model does quite well, and it also accurately predicts the cross sections for the hydrogen target and odd-numbered charge changes except for -1. Virtually every other predicted cross section departs significantly from the data. For all targets, the model predicts a larger-than-observed cross section for $\Delta Z=1$ and, with very few exceptions, smaller-than-observed cross sections over the rest of the ΔZ range. The discrepancies for the larger charge changes are often 50% or greater, which suggests that some model parameters need adjustment [22]. We note that the predicted cross sections do show an odd-even effect, which qualitatively agrees with the data.

(iii) The NUCFRG2 code [14], which is based on an abrasion-ablation fragmentation model. These predictions are shown as curves with small dashes. The model does well for the hydrogen data with $\Delta Z \geqslant 2$. We note too that the model accurately predicts the cross sections for the lead target at $\Delta Z=1$ and 2, whereas the predictions of models (i) and (ii) above are deficient. This may be due to the explicit inclusion in this code of electromagnetic dissociation cross sections, which are large in high-Z targets. For most of the other data, the predicted cross sections are 10–20 % larger than are observed. No odd-even effect is predicted, nor are the enhanced Si and Mg cross sections, although those are

---

[1]The scaling algorithm of Ref. [21] predicts cross sections for specific combinations of projectile, target, and fragment charges and masses. To facilitate comparisons with data and with other models, we used an isotope list generated by NUCFRG2 in order to determine which isotopes contribute significantly to the fragment production cross section at a given Z.
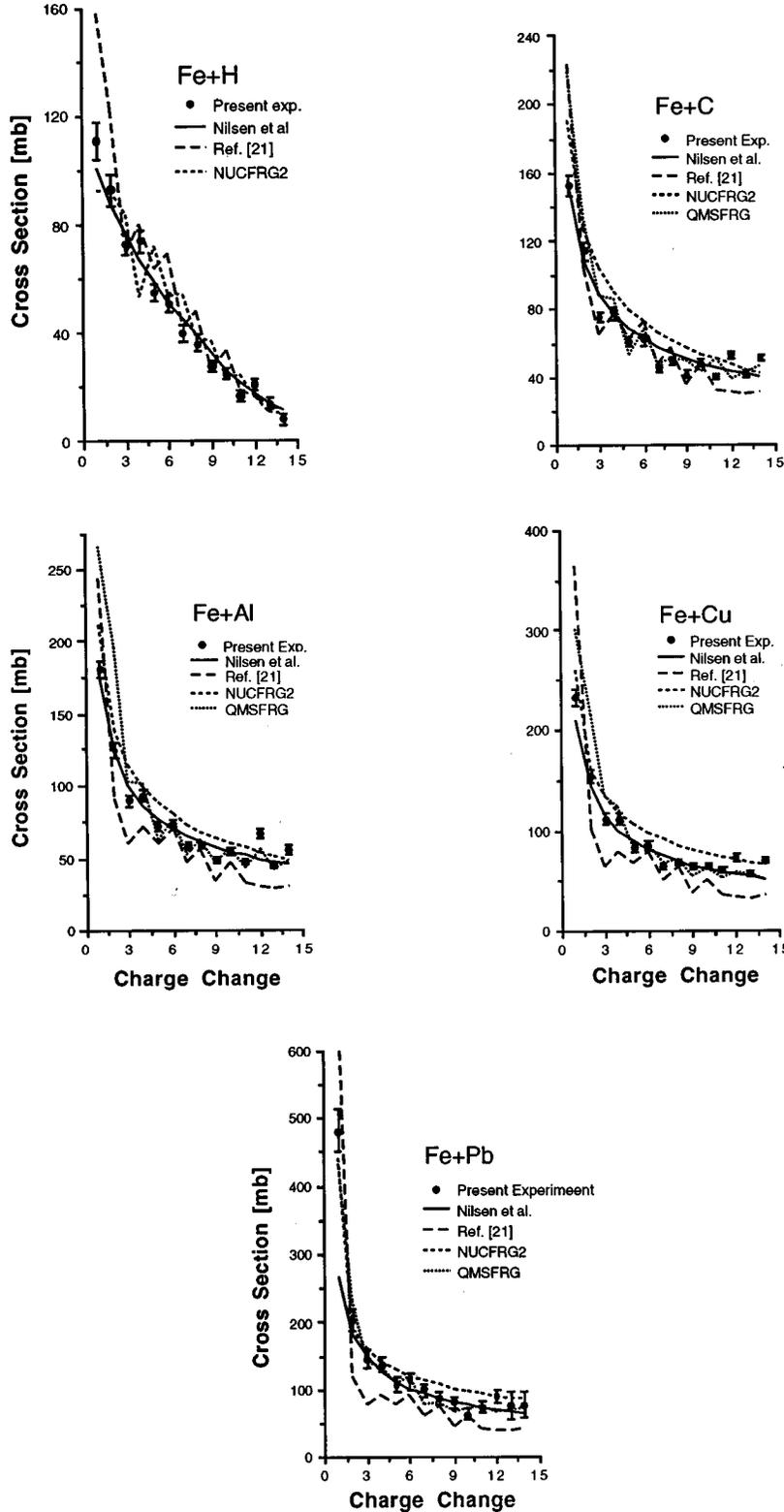
FIG. 3. Charge-changing cross sections for ΔZ from -1 to -14 for 1.05 GeV/nucleon ^{56}Fe incident on H, C, Al, Cu, and Pb targets. The solid lines are predictions from the parametrization of Nilsen et al. in Ref. [16]; the curves consisting of long dashes are predictions from the model of Ref. [21], the curves consisting of short dashes are predictions from the NUCFRG2 code [14], and the curves consisting of dots are predictions from the QMSFRG code [18].

(except for the Al target) in fairly good agreement with the data.

(iv) The quantum multiple scattering (QMSFRG) model [18], which is a reformulation of the abrasion-ablation physics used in NUCFRG2. The model does not, at present, calculate cross sections for hydrogen targets. These predictions are shown as curves with dots. For all targets, the model predicts an odd-even effect that follows the data well in the range from $\Delta Z = 4$ to $\Delta Z = 12$ (Si production). For C, Al, and Cu targets, the $\Delta Z \leq 3$ cross sections predicted by the model are far larger than are observed experimentally; the $\Delta Z = 1$ predictions tend to be high by roughly 40%. However, for Pb, the model does much better for small charge changes. We recall that, in Table II, the QMSFRG total charge-changing cross sections were seen to be systematically larger than the data by 5–10 %. Adjustments to the model which

TABLE X. Comparison of average differences (the $\Delta\sigma_{av}$ values) and rms's between the present experiment and several models.

Target	Nilsen *et al.*		Ref. [21]		NUCFRG2		QMSFRG	
	$\Delta\sigma_{av}$	rms	$\Delta\sigma_{av}$	rms	$\Delta\sigma_{av}$	rms	$\Delta\sigma_{av}$	rms
H	−0.010	0.11	0.15	0.21	0.002	0.24		
C	0.050	0.11	−0.051	0.22	0.19	0.14	0.077	0.17
Al	−0.030	0.11	−0.24	0.21	0.092	0.14	0.019	0.22
Cu	−0.066	0.10	−0.27	0.27	0.13	0.12	−0.002	0.18
Pb	−0.091	0.15	−0.30	0.27	0.12	0.17	−0.064	0.12

would reduce the $\Delta Z \leq 3$ cross sections would also significantly improve the agreement with the measured charge-changing cross sections; using a cluster model of the incident nucleus, rather than single-particle wave functions, is expected [23] to have precisely this effect, and will be implemented in future versions of the code.

In Table X, we again show ''average differences,'' here, with the model calculations playing the role of the σ_i (reported) in Eq. (6). Overall, the Nilsen *et al.* parametrization seems to best reproduce the cross sections, as both the averages and rms's are comparatively small. This is true in spite of the fact that the model misses some significant details apparent in the data, such as the odd-even effect. It is difficult to assess the physical meaning that may be carried by several of the parameters, and the authors of Ref. [16] state that many of the parameters are mutually correlated, further obscuring the physical interpretation. In contrast, both the NUCFRG and QMSFRG models have comparatively straightforward physical interpretations, and both reproduce the data at the 10–20 % level, albeit with somewhat larger rms's than were found for the Nilsen *et al.* parametrization. We note that none of the models predicts the enhanced cross sections that are seen for the production of silicon ($Z=14$) and magnesium ($Z=12$). We also note that all the models except NUCFRG2 show steadily decreasing values of $\Delta\sigma_{av}$ as target mass increases (for carbon and heavier targets).

D. Energy dependence of polyethylene cross sections

We have previously published data for the fragmentation of nominally 600 MeV/nucleon ^{56}Fe on polyethylene targets of various depths [24]. Owing to energy loss in materials upstream of the target, the energy at the target entrance for these data was 510 MeV/nucleon. The data were taken at the LBL Bevalac, and were initially presented as mean free paths and fragment fluences (with no corrections for multiple interactions). Using the methods outlined in Sec. III above, these data are readily converted to fragment production cross sections. Data from two targets were used, one 2-cm thick (1.84 g cm^{-2}), the other 5-cm thick (4.60 g cm^{-2}). For the 2-cm target, energy loss calculations show that the energy at target center was 481 MeV/nucleon; for the 5-cm target, 431 MeV/nucleon. The cross sections from the two data sets show no significant differences (implying that any energy dependence in this range is quite weak), and have therefore been combined. The total charge-changing cross section from these data is found to be 2890±65 mb at an average kinetic energy of 456 MeV/nucleon, where the error is the quadrature sum of statistical and systematic contributions. In Ref. [6], Webber *et al.* find a cross section of 2917±29 mb

at 434 MeV/nucleon, in good agreement with our result at a very similar energy. We find a cross section of 2818±6 ±70 mb at 1.05 GeV/nucleon, while Webber *et al.* find 2962±44 mb at 1.086 GeV/nucleon and Westfall *et al.* find 2920±94 mb at 1.88 GeV/nucleon. These are all, within the errors, consistent with little or no energy dependence of the charge-changing cross section for iron on polyethylene for beam energies between approximately 0.5 and 2 GeV/nucleon.

The fragment production cross sections are shown in Table XI, along with the cross sections as determined from the 1.05 GeV/nucleon data. The comparison is complicated by the fact that, in the earlier, lower-energy experiment, the angular acceptance was somewhat smaller, only 1.6°. The cross sections have been corrected for acceptance assuming the fragments follow Gaussian transverse-momentum distributions as specified in Ref. [13]. (We set the parameter $\sigma_{0,\text{expt}}=110$ MeV/c.) The largest correction, for $Z=13$, is 21%, or 10 mb. For $Z \geq 23$, we find the 600 MeV/nucleon cross sections are systematically larger than those at 1.05 GeV/nucleon, although the errors are sufficiently large to preclude any definitive statement. For $Z \leq 19$, the 600 MeV/nucleon cross sections are systematically smaller than the corresponding cross sections at the higher beam energy. This is qualitatively consistent with the trend seen in the Webber

TABLE XI. Cross sections for iron on polyethylene at two beam energies. The 456 MeV/nucleon data are derived from previously published fragment fluence data. For comparison, the results of Webber *et al.* at very similar energies are shown.

	σ(mb) 1.05 GeV/nucleon	σ(mb) 456 MeV/nucleon	σ(mb) Webber 1086 MeV/nucleon	σ(mb) Webber 434 MeV/nucleon
σ_{25}	374±12	389±30	378±7	504±9
σ_{24}	299±10	328±25	287±5	432±8
σ_{23}	220±8	245±22	211±7	296±10
σ_{22}	225±8	224±21	217±7	286±9
σ_{21}	170±6	169±13	159±5	196±6
σ_{20}	164±6	164±13	161±5	167±5
σ_{19}	125±5	110±11	112±7	95±5
σ_{18}	121±5	102±9	109±7	87±5
σ_{17}	97±4	73±8	80±5	53±3
σ_{16}	98±4	86±8	95±6	60±4
σ_{15}	74±3	61±6	59±7	33±3
σ_{14}	92±4	59±8	83±9	60±5
σ_{13}	70±3	56±5	53±6	

et al. data (also shown in Table XI): with increasing beam energy, cross sections for larger ΔZ increase, while those for small ΔZ decrease, so that the sum is (approximately) constant. However, Webber *et al.* report a much larger effect than is seen in our data.

VII. CONCLUSIONS

We have measured the charge-changing and fragment production cross sections for 1.05 GeV/nucleon ^{56}Fe ions in several elemental targets and polyethylene. The charge-changing cross sections have been measured with a systematic error estimated to be 2.5%, and the fragment cross sections roughly 4%. The charge-changing cross sections are seen to be reasonably well modeled by an energy-independent parametrization, and also by a semiempirical abrasion-ablation model. The fragment production cross sections were found for the most part to lie between the higher values of Westfall *et al.* and the lower values found by Cummings *et al.*, and to be in better agreement with the latter. The fragment production cross sections were compared to four models, none of which accurately reproduced all of the

important features of the data, which suggests that further refinements are in order. Finally, the fragment production cross sections on polyethylene were compared to those obtained at a lower beam energy and found to show a trend similar to that reported by Webber *et al.*, although the quantitative agreement between experiments is not good at the lower energy.

[1] C.-X. Chen *et al.*, Phys. Rev. C **49**, 3200 (1994).

[2] J. W. Wilson, M. Kim, W. Schimmerling, F. F. Badavi, S. A. Thibeault, F. A. Cucinotta, J. L. Shinn, and R. Kiefer, Health Phys. **68**, 50 (1995).

[3] J. A. Simpson, in *Composition and Origin of Cosmic Rays*, edited by M. M. Shapiro (Reidel, Dordrecht, 1983), p. 1.

[4] G. D. Westfall, L. W. Wilson, P. J. Lindstrom, H. J. Crawford, D. E. Greiner, and H. H. Heckman, Phys. Rev. C **19**, 1309 (1979).

[5] V. E. Dudkin, E. E. Kovalev, N. A. Nefedov, V. A. Antonchik, S. D. Bogdanov, V. I. Ostroumov, H. J. Crawford, and E. V. Benton, Nucl. Phys. **A509**, 783 (1990).

[6] W. R. Webber, J. C. Kish, and D. A. Schrier, Phys. Rev. C **41**, 520 (1990).

[7] W. R. Webber, J. C. Kish, and D. A. Schrier, Phys. Rev. C **41**, 533 (1990).

[8] W. R. Webber, J. C. Kish, and D. A. Schrier, Phys. Rev. C **41**, 547 (1990).

[9] J. R. Cummings, W. R. Binns, T. L. Garrard, M. H. Israel, J. Klarmann, E. C. Stone, and C. J. Waddington, Phys. Rev. C **42**, 5208 (1990).

[10] V. E. Dudkin, E. E. Kovalev, N. A. Nefedov, V. A. Antonchik, S. D. Bogdanov, V. F. Kosmach, A. Yu. Likhachev, J. Hassan, E. V. Benton, and H. J. Crawford, Nucl. Phys. **A568**, 906 (1994).

[11] C. J. Zeitlin, K. A. Frankel, W. Gong, L. Heilbronn, E. J. Lampo, R. Leres, J. Miller, and W. Schimmerling, Radiat. Meas. **23**, 65 (1994).

[12] A. S. Goldhaber, Phys. Lett. **53B**, 306 (1974).

[13] R. K. Tripathi and L. W. Townsend, Phys. Rev. C **49**, 2237 (1994).

[14] J. W. Wilson, J. L. Shinn, L. W. Townsend, R. K. Tripathi, F. F. Badavi, and S. Y. Chun, Nucl. Instrum. Methods Phys. Res. B **94**, 95 (1994).

[15] L. W. Townsend and J. W. Wilson, Radiat. Res. **106**, 283 (1986).

[16] B. S. Nilsen, C. J. Waddington, J. R. Cummings, T. L. Garrard, and J. Klarmann, Phys. Rev. C **52**, 3277 (1995).

[17] H. C. Bradt and B. Peters, Phys. Rev. **77**, 54 (1950).

[18] F. A. Cuccinotta, J. W. Wilson, R. K. Tripathi, and L. W. Townsend, Adv. Space Res. (in press).

[19] C. N. Knott *et al.*, Transport Collaboration, Phys. Rev. C **53**, 347 (1996).

[20] L. W. Townsend, F. A. Cuccinotta, and J. W. Wilson, in *Biological Effects and Physics of Solar and Galactic Cosmic Rays*, edited by C. E. Swenberg, G. Horneck, and G. Stassinopoulos (Plenum, New York, 1993), pp. 787–810.

[21] C. H. Tsao, R. Silberberg, A. F. Barghouty, L. Sihver, and T. Kanai, Phys. Rev. C **47**, 1257 (1993).

[22] A. F. Barghouty (private communication).

[23] J. W. Wilson (private communication).

[24] C. Zeitlin, J. Miller, L. Heilbronn, K. Frankel, W. Gong, and W. Schimmerling, Radiat. Res. **145**, 655 (1995).